Stimulated vacuum emission and photon absorption in strong electromagnetic fields

I. A. Aleksandrov[1,2] A. Di Piazza,[3] G. Plunien,[4] and V. M. Shabaev[1]

[1]*Department of Physics, Saint Petersburg State University,*
Universitetskaya Naberezhnaya 7/9, Saint Petersburg 199034, Russia
[2]*Ioffe Institute, Politekhnicheskaya street 26, Saint Petersburg 194021, Russia*
[3]*Max Planck Institute for Nuclear Physics, Saupfercheckweg 1, Heidelberg D-69117, Germany*
[4]*Institut für Theoretische Physik, TU Dresden, Mommsenstrasse 13, Dresden D-01062, Germany*

According to quantum electrodynamics (QED), a strong electromagnetic field can make the vacuum state decay via the production of electron-positron pairs. Here we investigate the emission of soft photons which accompanies a nonperturbative process of pair production. Our analysis is carried out within the Furry picture to first order in the fine-structure constant. Also, it is shown that the presence of photons in the initial state gives rise to an additional (stimulated) channel of photon emission besides the pure vacuum one. On the other hand, the number of final (signal) photons includes also a negative contribution due to photon absorption within the pair production process. These contributions are evaluated and compared. To obtain quantitative predictions in the domain of realistic field parameters, we employ the Wentzel-Kramers-Brillouin approach. We propose using an optical-probe photon beam, whose intensity changes as it traverses a spatial region where a strong electric component of a background laser field is present. It is demonstrated that relative intensity changes on the level of 1% can be experimentally observed once the intensity of the strong background field exceeds 10^{27} W/cm^2 within a large laser-wavelength interval. This finding is expected to significantly support possible experimental investigations of nonlinear QED phenomena in the nonperturbative regime.

I. INTRODUCTION

As early as the 1930s [1–3], it became evident that the quantum nature of the electromagnetic interaction manifests itself in an effective violation of the superposition principle taking place in the classical theory based on Maxwell's equations in vacuum. It was found that Maxwell's Lagrangian gains additional quantum corrections which lead to remarkable nonlinear phenomena such as light-by-light scattering [1–4] and Sauter-Schwinger electron-positron pair production [2,5,6] (for review, see, e.g., Refs. [7–15]). To galvanize the quantum fluctuations, one basically strives to make them interact with a strong background field. In this context, the rapid developments of the technology for generating high-power laser pulses has continuously encouraged active theoretical and experimental research. Although some of the nonlinear phenomena of strong-field quantum electrodynamics (QED) were already

practically observed [16–19], the nonperturbative process of electron-positron pair production, i.e., the Sauter-Schwinger effect, is still experimentally unexplored. Whereas one can investigate analogous phenomena in condensed matter systems (see, e.g., Refs. [20–27]), in standard QED the Sauter-Schwinger mechanism is exponentially suppressed unless the electric-field strength approaches the critical value $E_c = m^2 c^3/(|e|\hbar) \approx 1.3 \times 10^{16}$ V/cm (m and $e < 0$ are the electron mass and charge, respectively). This corresponds to an intensity of 2.3×10^{29} W/cm^2, while the maximum intensity achieved so far amounts to 10^{23} W/cm^2 [28].

As was proposed in Ref. [29], one can attempt to experimentally study the process of vacuum photon emission accompanying the Sauter-Schwinger mechanism as illustrated in Fig. 1. Measuring this additional radiation would allow one to indirectly probe nonperturbative pair production. This vertex diagram exactly incorporates the interaction with the classical electromagnetic background, which is reflected by the double fermionic lines. The process described by the diagram is of the first order in the fine-structure constant $\alpha = e^2/(4\pi\hbar c)$ and predicts emission of a huge number of soft photons [29–31]. In the present study, we revisit the quantitative features of this
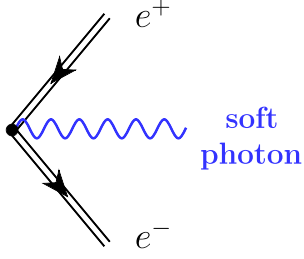
FIG. 1. Vertex diagram describing vacuum emission of soft photons accompanying the Sauter-Schwinger effect. The double lines represent the exact electron wave function in the presence of the external field, i.e., the external classical background is treated nonperturbatively.

phenomenon providing closed-form expressions and numerical estimates describing the number density of photons emitted in the domain of realistic field parameters. Furthermore, we propose another experimental scenario which is closely related to vacuum photon emission but involves additional (probe) photons already in the initial state. It turns out that the presence of these photons induces two additional contributions besides the purely vacuum one discussed above. One of them is exactly the same diagram as that displayed in Fig. 1 with the outgoing-photon state coinciding with that of the initial (probe) photon. The other contribution is negative and describes the absorption of the initial photon with the production of an electron-positron pair. As will be shown in what follows, the sum of these two photon-induced terms can lead to notable change of the probe beam intensity. Measuring this change is another tool for investigating the Sauter-Schwinger mechanism in the experiment. In this paper, we argue that this scenario proves to be more favorable than measuring the vacuum radiation itself or detecting pairs directly since the probe-beam technique corresponds to a lower threshold with respect to the laser intensity.

Since we are interested in the nonperturbative regime, the interaction with the classical external field is taken into account exactly, i.e., we work within the Furry picture. The quantized part of the electromagnetic field is treated within perturbation theory (PT). To compute the Feynman diagrams, we first employ our numerical technique developed previously in the context of pair production [32–34] and subsequently generalized for studying radiative processes [31]. Second, we also perform calculations using perturbation theory with respect to the classical background in order to benchmark our nonperturbative numerical procedures. Finally, to obtain quantitative predictions in the domain of realistic field parameters, we construct the necessary wave functions by means of the Wentzel-Kramers-Brillouin (WKB) approach and complete the evaluation of the diagrams analytically. The closed-form final expressions are then used to examine the experimental feasibility of our proposal.

The paper has the following structure. In Sec. II we recap the main general features of vacuum photon emission. In Sec. III we discuss the photon-induced contributions in the case of one initial photon or many identical photons. Moving on to specific calculations, in Sec. IV we first describe our nonperturbative procedure in more detail and then employ PT to benchmark our technique. In Sec. V we examine the photon emission process within the framework of scalar QED. In Sec. VI we perform WKB calculations and obtain closed-form expressions for the necessary quantities. The experimental prospects of our proposal as well as the feasibility of measuring the vacuum radiation and Sauter-Schwinger mechanism itself are discussed in Sec. VII. Finally, we conclude in Sec. VIII. We will employ the units $\hbar = c = 1$.

II. VACUUM PHOTON EMISSION WITHIN THE FURRY PICTURE

In our study, the external classical field is treated nonperturbatively, i.e., within the Furry picture. The quantized electron-positron field ψ interacts with both the classical background $\mathcal{A}^\mu$ and quantized part of the electromagnetic field $\hat{A}^\mu$. The photons emitted, as well as the probe photons, are quanta of the latter. The quantized part is incorporated by PT within the interaction picture [35]. The corresponding S operator has the form

$$S = T \exp\left(-i \int d^4 x j^\mu(x) \hat{A}_\mu(x)\right), \quad (1)$$

where $x = (t, \boldsymbol{x})$, T is the time-ordering operator, and j^μ is a current operator in the presence of the external background $\mathcal{A}^\mu$. The external field strength is assumed to vanish outside the interval $t \in [t_{\text{in}}, t_{\text{out}}]$, and in Eq. (1) one integrates over this temporal region. In our case the field is switched on and off adiabatically, so we will imply $t_{\text{in/out}} \to \mp \infty$.

The quantized part of the electromagnetic field has the following standard decomposition in terms of the photon mode functions,

$$\hat{A}_\mu(x) = \sum_{\lambda=0}^{3} \int d\boldsymbol{k} [c_{\boldsymbol{k},\lambda} f_{\boldsymbol{k},\lambda,\mu}(x) + c_{\boldsymbol{k},\lambda}^\dagger f_{\boldsymbol{k},\lambda,\mu}^*(x)], \quad (2)$$

where $c_{\boldsymbol{k},\lambda}^\dagger$ and $c_{\boldsymbol{k},\lambda}$ are the photon creation and annihilation operators, respectively, and $f_{\boldsymbol{k},\lambda,\mu}(x) = (2\pi)^{-3/2} (2k^0)^{-1/2} \times$ $e^{-ikx} \varepsilon_\mu(\boldsymbol{k}, \lambda)$ is the photon wave function corresponding to momentum $\boldsymbol{k}$ ($k^0 = |\boldsymbol{k}|$) and polarization λ. The electron-positron field operator ψ can be decomposed either in terms of the so-called *in* one-particle solutions $_{\pm}\varphi_n(x)$ or in terms of the *out* solutions $^{\pm}\varphi_n(x)$. The *in* (*out*) wave functions are determined by their asymptotic form for $t \leq t_{\text{in}}$ ($t \geq t_{\text{out}}$), where they have a well-defined sign of energy denoted by $\pm$. The quantum number n incorporates momentum and spin. In what follows, we will need the expansion of the

electron-positron field operator in terms of the *in* solutions of the Dirac equation,

$$\psi(x) = \sum_n [a_{n+}\varphi_n(x) + b_{n-}^\dagger \varphi_n(x)], \qquad (3)$$

where we have introduced the electron (positron) creation and annihilation operators $a_n^\dagger$ ($b_n^\dagger$) and a_n (b_n), respectively. These operators obey the usual anticommutation relations. The vacuum state will be denoted by $|0, \text{in}\rangle$. The current operator involved in Eq. (1) can now be constructed via $j^\mu(x) = (e/2)[\bar\psi(x)\gamma^\mu, \psi(x)]$.

In this section we assume that the initial state is a pure vacuum one, i.e., we do not introduce any additional photons, $|\text{in}\rangle = |0, \text{in}\rangle$. To describe the process of photon emission, we will evaluate the number density of photons in the final state, which can be obtained by evolving $|0, \text{in}\rangle$ with the aid of the S operator (1),

$$n_{\boldsymbol{k},\lambda}^{(\text{vac})} = \langle 0, \text{in}|S^\dagger c_{\boldsymbol{k},\lambda}^\dagger c_{\boldsymbol{k},\lambda} S|0, \text{in}\rangle. \qquad (4)$$

Note that this quantity is an inclusive observable, i.e., the final state is not specified here and it may contain an arbitrary number of pairs. The "mean number" $n_{\boldsymbol{k},\lambda}^{(\text{vac})}$ represents the number density of photons in the momentum space, $n_{\boldsymbol{k},\lambda}^{(\text{vac})} = dN_{\boldsymbol{k},\lambda}^{(\text{vac})}/d\boldsymbol{k}$. In the present study, we evaluate Eq. (4) to first order in the fine-structure constant using the series expansion of the exponential (1). Straightforward calculations yield [31]

$$n_{\boldsymbol{k},\lambda}^{(\text{vac})} = \left| \int d^4x\, j_{\text{in}}^\mu(x) f_{\boldsymbol{k},\lambda,\mu}^*(x) \right|^2$$
$$+ e^2 \sum_{n,m} \left| \int d^4x\, {}_+\bar\varphi_n(x)\gamma^\mu f_{\boldsymbol{k},\lambda,\mu}^*(x)\, {}_-\varphi_m(x) \right|^2, \quad (5)$$

where $j_{\text{in}}^\mu(x) = \langle 0, \text{in}|j^\mu(x)|0, \text{in}\rangle$ is the vacuum current. This expression can also be derived by computing transition amplitudes and summing over the possible final states containing various numbers of electrons and positrons. This alternative, if tedious, scheme is presented in Ref. [35].

The first term in Eq. (5) corresponds to the so-called tadpole (reducible) contribution explored in numerous studies (see, e.g., Refs. [30,31,35–45]). It predicts the emission of photons similar to those constituting the external field or higher harmonics. The most robust technique for computing this term is based on the locally-constant field approximation (LCFA) [38–41,43,44]. This technique is expected to be accurate once the external-field frequency ω is much less than m, which was evidently confirmed in our recent investigation [31], where it was also shown that the LCFA prediction may considerably differ from the exact values of the photon yield if $(\omega/m)^2 \gtrsim 0.3$. Recently, it was also shown that high harmonic generation can be addressed by inspecting the conduction and polarization currents

within the kinetic approach [45] (see also Ref. [46], where most general kinetic equations were obtained starting from nonequilibrium QED).

In this study, we focus on the process of soft photon emission accompanying the Sauter-Schwinger mechanism of pair production. This process is described by the second term in Eq. (5), which can be illustrated by the vertex diagram in Fig. 1. Since it is responsible for the low-energy part of the radiation spectrum, we refrain from discussing the tadpole contributions in what follows. In Ref. [29] the vertex diagram was examined in the case of a spatially uniform external background. Recently [31], it was demonstrated that taking into account the spatiotemporal inhomogeneities of the external field in the case of a standing electromagnetic wave leads to a notable anisotropy of the emitted photons providing additional signatures that can be, in principle, measured in the experiment.

Here we will also assume that the external field does not depend on the spatial coordinates, $\mathcal{A}^\mu = \mathcal{A}^\mu(t)$. This will allow us to obtain relatively simple estimates approximating a combination of two counterpropagating (high-intensity) laser pulses in the vicinity of a maximal electric field amplitude by a uniform background. As was shown in Refs. [29,31], the photon number density for low energies $k_0 \ll m$ is proportional to $1/k_0^3$. In the case of a spatially homogeneous field, Eq. (5) yields factor V, the volume of the system, so we isolate it and present the photon number density in the following form,

$$\frac{n_{\boldsymbol{k},\lambda}^{(\text{vac})}}{V} = \frac{A_{\boldsymbol{n},\lambda}}{k_0^3} + \frac{B_{\boldsymbol{n},\lambda}}{k_0^2} + \cdots, \qquad (6)$$

where $\boldsymbol{n} = \boldsymbol{k}/k_0$, i.e., the coefficients $A_{\boldsymbol{n},\lambda}$ and $B_{\boldsymbol{n},\lambda}$ depend on the photon polarization λ and the propagation direction. Note that although the photon number density diverges as $k_0 \to 0$, the energy emitted is finite. The function $f_\gamma(\boldsymbol{k})$ introduced in Ref. [29] corresponds to the sum of Eq. (6) over λ. In quantitative estimates, the interaction volume V is treated as a volume of the focal spot of laser radiation. The experimental prospects will be discussed in detail in Sec. VII.

One might also ask whether it is necessary to take into account the vertex diagram in Fig. 1 when computing the number of electron-positron pairs. In this case, one has to integrate over the photon momentum $\boldsymbol{k}$, which leads to an infrared divergence. However, according to Ref. [47], the divergent higher-order contributions, in fact, do not affect the leading-order result (see also Ref. [48]; this issue was examined in the context of other nonperturbative processes in, e.g., Refs. [49–51]). The same holds true with regard to radiative corrections to the process of soft-photon emission considered in the present study. As we always specify the signal photon energy $k_0 > 0$, the leading contribution (6) is finite, whereas the higher-order infrared divergences are irrelevant. On the other hand, the number of photons can be

affected by higher-order diagrams where multiple k_0-quanta are emitted simultaneously. Nevertheless, these corrections are small since they are suppressed by powers of $\alpha \ln(m/k_0)$ [47,48]. In what follows, we will assume that $k_0 \geq 10^{-6}m$, which leads to $\alpha \ln(m/k_0) < 0.1$, so the higher-order terms will be disregarded.

III. ADDITIONAL PHOTONS IN THE INITIAL STATE

In this section we will analyze the process of photon emission in the presence of additional (probe) photons in the initial state, which were absent in the vacuum state $|0, \text{in}\rangle$ considered previously.

A. One-photon state

Consider now a one-photon state $|\text{in}\rangle = c_{\boldsymbol{q},\varkappa}^{\dagger}|0, \text{in}\rangle$. Calculating the photon number density to first order in α via

$$n_{\boldsymbol{k},\lambda}^{(1)} = \langle 0, \text{in}|c_{\boldsymbol{q},\varkappa}S^{\dagger}c_{\boldsymbol{k},\lambda}^{\dagger}c_{\boldsymbol{k},\lambda}Sc_{\boldsymbol{q},\varkappa}^{\dagger}|0, \text{in}\rangle, \qquad (7)$$

one obtains a sum of two contributions. The first one is exactly $n_{\boldsymbol{k},\lambda}^{(\text{vac})}$ given in Eq. (5). Note that this part does not involve the quantum numbers of the probe photon. The second contribution to $n_{\boldsymbol{k},\lambda}$ appears due to the presence of the additional photon and represents the difference shown in Fig. 2. The photon wave functions correspond to the quantum numbers $\boldsymbol{q}$ and $\varkappa$ of the initial photon, so these terms contribute only when $\boldsymbol{k}$, λ coincide with $\boldsymbol{q}$, $\varkappa$. Together with the process without additional quanta, the three parts can be interpreted as spontaneous emission, stimulated emission, and photon absorption, respectively, similar to the atomic physics notions. To properly treat the "resonance" character of the photon-induced terms, one should introduce a smearing function for the initial photon state. We assume that it is localized in a small vicinity of $\boldsymbol{q}$ which has volume V_q (in momentum space). Another important point is the fact that the difference between the two diagrams in Fig. 2 appears due to complex conjugation of the photon wave function, which is equivalent to the substitution $k^{\mu} \rightarrow -k^{\mu}$. It means that the second diagram in
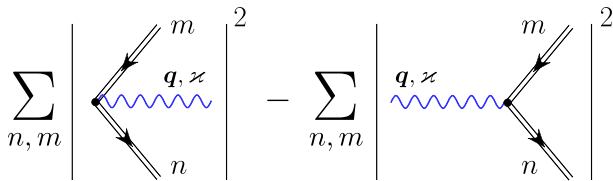

FIG. 2. Two additional contributions which appear in the case of a one-photon initial state. The sum over the final fermionic states involves integration over momentum and summation over spin. The photon lines correspond to the quantum numbers $\boldsymbol{q}$ and $\varkappa$ of the initial photon.

Fig. 2 (photon absorption) has the same behavior (6) with the opposite sign of the $1/k_0^2$ term. One factor $1/k_0$ relates to the normalization of the photon wave functions, so one should change the sign of the even powers. Whereas the difference in Fig. 2 no longer has the $1/k_0^3$ term, the next-to-leading-order term doubles. Note that there are no stimulated tadpole contributions, which is no surprise as the vacuum current is real, so conjugating the photon wave function, one does not change the absolute value of the diagram.

We assume that the probe photons will be measured within the whole V_q region, i.e., we integrate the photon number density over the small momentum volume, where the initial photon was localized. It brings us to the following number of photons ($\boldsymbol{l} = \boldsymbol{q}/q_0$),

$$N^{(1)} = 1 + \left(\frac{A_{l,\varkappa}}{q_0^3} + \frac{B_{l,\varkappa}}{q_0^2} + \cdots\right)VV_q + \frac{2(2\pi)^3 B_{l,\varkappa}}{q_0^2} + \cdots. \qquad (8)$$

Here the first term corresponds to the trivial zeroth-order contribution and merely indicates that the initial state contains one photon. The second vacuum term is enhanced by the large factor V since the vacuum emission takes part in the whole interaction region. On the other hand, it is suppressed by V_q since we have integrated only over this small momentum region. In the quantitative estimates concerning this vacuum term, we will take into account that this radiation is emitted at all the other directions (see Sec. VII). The vacuum contribution is essentially determined by the first term in parentheses in Eq. (8). Finally, the last term in Eq. (8) comes from the difference in Fig. 2 and governs the photon-induced contribution. Here the factor 2 appears since the B term doubles in the difference of the two Feynman diagrams. Let us briefly discuss the origin of the factor $(2\pi)^3$. When introducing a photon smearing function, one has to perform two additional integrations in Eq. (7). Assuming that the smearing function is equal to some constant C in a small vicinity of momentum $\boldsymbol{q}$, one can simply multiply the integrand by factor V_q^2 and replace the smearing function with C. This leads to an overall factor $C^2 V_q^2$. Since the initial state contains one quantum, the zeroth-order photon number density integrated over V_q yields unity, i.e., $C^2 V_q = 1$. The external field is homogeneous in space, so the number density will be proportional to the volume V as in Eq. (6). However, here V is determined by the spatial volume occupied by the initial photon, i.e., V should be replaced with $(2\pi)^3/V_q$. Accordingly, we arrive at the factor $(2\pi)^3$ in the last term in Eq. (8). Note that unlike the vacuum contribution, this one is enhanced once the initial state contains many probe photons. This will be discussed next.

B. *N*-photon state

The stimulated emission and absorption parts give rise to the number of signal photons corresponding to the third term in Eq. (8). It is not enhanced by V since the probe photon does not "feel" the boundaries of the interaction region. However, the crucial point is that in the case of N photons in the initial state, this term will be proportional to N, which can be verified by direct calculations of the mean number density of photons as was discussed above. Accordingly, the photon-induced contribution yields

$$N^{(\text{ph})} = \frac{2(2\pi)^3 |B_{l,\varkappa}|}{q_0^2} N. \tag{9}$$

As will be seen later, the coefficient $B_{l,\varkappa}$ can be positive or negative depending on the field configuration, i.e., the dominant contribution can arise from either the process of stimulated emission or from the absorption channel.

Here we propose to measure the relative change of the optical probe beam intensity given by the ratio $N^{(\text{ph})}/N$. In Sec. VII we will assess this scenario together with the proposal to detect the vacuum radiation and with possible observations of the pair production process. In order to provide quantitative estimates and discuss the feasibility of measuring the signal experimentally, one should evaluate the coefficients $A_{n,\lambda}$ and $B_{n,\lambda}$. This will be a subject of the following sections.

IV. FURRY-PICTURE CALCULATIONS VERSUS PERTURBATION THEORY

In this section we will perform numerical calculations of the coefficients $A_{n,\lambda}$ and $B_{n,\lambda}$ and benchmark the results by means of PT. In what follows, the external background is assumed to be a Sauter pulse

$$E_z(t) = \frac{E_0}{\cosh^2(t/\tau)}, \tag{10}$$

so the classical potential reads

$$\mathcal{A}^3(t) = -E_0\tau \tanh(t/\tau). \tag{11}$$

The other components vanish. We also introduce $\mathcal{A}_0 \equiv \mathcal{A}^3(+\infty) = -E_0\tau$ and $\boldsymbol{\mathcal{A}}_0 = \mathcal{A}_0 \boldsymbol{e}_z$.

A. Nonperturbative calculations

To calculate the coefficients $A_{n,\lambda}$ and $B_{n,\lambda}$, one has to compute the second term in Eq. (5). Since the external field does not depend on the spatial coordinates, the in solutions involved in Eq. (5) can be represented as

$$_\zeta\varphi_{\boldsymbol{p},s}(x) = (2\pi)^{-3/2}e^{i\zeta\boldsymbol{p}\boldsymbol{x}} {}_\zeta\chi_{\boldsymbol{p},s}(t), \tag{12}$$

where $\zeta = \pm$ and $s = \pm 1$ defines the spin state. Then the vacuum contribution to the number density of soft photons takes the following form [29,31],

$$\frac{(2\pi)^3}{V} n_{\boldsymbol{k},\lambda}^{(\text{vac})} = \frac{\alpha}{4\pi^2}\frac{1}{k_0}\sum_{s,s'}\int d\boldsymbol{p}\left|\int dt_+\bar{\chi}_{\boldsymbol{p},s}(t)\gamma^\mu\varepsilon_\mu^*(\boldsymbol{k},\lambda)_-\chi_{-\boldsymbol{p}-\boldsymbol{k},s'}(t)e^{ik_0t}\right|^2. \tag{13}$$

When integrating over $t \in (-\infty, t_{\text{in}}]$ and $t \in [t_{\text{out}}, +\infty)$, one has to introduce a factor $e^{-\varepsilon|t|}$ ($\varepsilon \to 0$). In fact, the leading contribution $A_{n,\lambda}/k_0^3$ arises from the region $[t_{\text{out}}, +\infty)$ [29], so one does not need to perform numerical integration over the intermediate time domain. Moreover, the coefficient $A_{n,\lambda}$ can be evaluated analytically (see Appendix A),

$$A_{n,\lambda} = \frac{\alpha}{4\pi^5}\int d\boldsymbol{p}\,\frac{(\boldsymbol{P},\boldsymbol{e}_\lambda)^2 p_0^2(\boldsymbol{P})}{[p_0^2(\boldsymbol{P}) - (\boldsymbol{P},\boldsymbol{n})^2]^2}\,n_{\boldsymbol{p}}(1 - n_{\boldsymbol{p}}), \tag{14}$$

where $\boldsymbol{P} \equiv \boldsymbol{p} - e\boldsymbol{\mathcal{A}}_0$, $p_0(\boldsymbol{p}) \equiv \sqrt{m^2 + \boldsymbol{p}^2}$, and $\boldsymbol{e}_\lambda$ is a three-dimensional photon polarization vector. To derive expression (14), we have employed the explicit formulas for the one-particle transitions, which can be obtained in the case of the Sauter pulse (10) since the Dirac equation can be solved analytically [35,52]. The number density $n_{\boldsymbol{p}}$ of the electrons produced is also known exactly [35,52,53].

Note that this quantity does not depend on spin s and never exceeds unity.

To evaluate the coefficient $B_{n,\lambda}$, we use the general expression (13) and subtract the term with the opposite sign of k^μ from the $\boldsymbol{p}$ integrand and then divide the result by 2.

B. Perturbation theory

We also employ a PT approach to test our nonperturbative procedure. The leading contribution of the vertex diagram can be evaluated as displayed in Fig. 3. The ordinary thin lines correspond here to the free solutions of
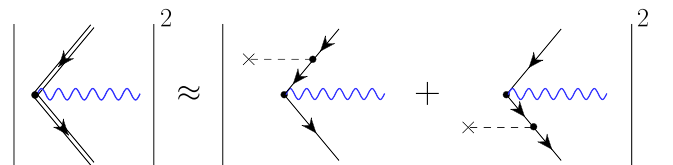

FIG. 3. Perturbative expansion of the vertex diagram.

the Dirac equation or to the free propagator in the case of the internal line. The crosses denote the interaction with the classical background $\mathcal{A}^\mu$.

Computing directly the Feynman diagrams in Fig. 3, we arrive at

$$A_{n,\lambda}^{(PT)} = \frac{\alpha}{4\pi^3}(eE_0\tau^2)^2 \int d\boldsymbol{p} \frac{1}{\sinh^2(\pi\tau p_0)} \frac{(\boldsymbol{p},\boldsymbol{e}_\lambda)^2(p_0^2 - p_z^2)}{[p_0^2 - (\boldsymbol{p},\boldsymbol{n})^2]^2},$$
(15)

where $p_0 = p_0(\boldsymbol{p}) = \sqrt{m^2 + \boldsymbol{p}^2}$. This expression coincides with the leading term of the perturbative expansion of Eq. (14), as it should. To calculate $B_{n,\lambda}$, we utilize the subtraction procedure as described in the previous section. The PT approach is only accurate if $|eE_0|\tau \ll m$, i.e., the so-called Keldysh parameter $\gamma = m/(|eE_0|\tau)$ is sufficiently large, which is obviously not a realistic condition. For this reason, one has to perform nonperturbative calculations as was stated above.

However, to benchmark our exact numerical approach, we compare the results with the PT predictions. As an example, in Fig. 4 we display the coefficients $A_{n,\lambda}$ and $B_{n,\lambda}$ for $\boldsymbol{n} = \boldsymbol{e}_y$ and photon polarization along the z axis, $\boldsymbol{e}_\lambda = \boldsymbol{e}_z$ (we use index yz). The coefficients are presented as functions of E_0 for $\tau = 1.0m^{-1}$. We observe that the PT approach provides quite accurate predictions for sufficiently weak pulses.

Finally, we point out that unlike the PT approach, one cannot employ the LCFA as it is not suitable for computing the number density of soft photons. In fact, one usually utilizes the LCFA, for instance, to describe the nonlinear Breit-Wheeler mechanism of high-energy photon decay in strong external fields. Note that according to Refs. [54,55], in the case of a plane wave background the second diagram in Fig. 2 is exponentially suppressed. The first diagram in

Fig. 2 does not even contribute in a plane wave in accordance with the fact that plane waves do not produce pairs. Our direct nonperturbative calculations, taking into account the temporal dependence of the external field, capture the effect of interest unlike the LCFA. To incorporate spatial inhomogeneities, one should either evaluate diagrams in the presence of spacetime-dependent fields, which is a formidable task, or sum the results over the spatial profile according to the local approximation employed in Ref. [31] (see also Ref. [56]). However, here we assume the field to be spatially uniform to save computational time and obtain the necessary estimates. The spatial finiteness of the interaction region is taken into account by the volume factor V as will be discussed in Sec. VII.

V. PHOTON EMISSION IN SCALAR QED

Since we are interested in computing the coefficients $A_{n,\lambda}$ and $B_{n,\lambda}$ for more realistic parameters of the external field, it is possible to simplify calculations by using the WKB approach. This is particularly important for calculating $B_{n,\lambda}$ as in this case, we do not have a closed-form expression like Eq. (14). As we assume that the external field is linearly polarized and spatially homogeneous, the spin effects should be insignificant, which allows one to consider scalar QED, where the calculations are simpler. The result will be multiplied by a factor of 2. Note that the total particle yield in spinor and scalar QED can possess different quantitative patterns also due to effects of statistics [57] if the number density of particles produced is sufficiently large. However, these effects come into play only for $E_0 \gtrsim E_c$, so here they can be completely disregarded (the number density n_p in the results presented below is always less than 10^{-6}). Let us now rigorously compute the coefficients $A_{n,\lambda}$ within scalar QED.

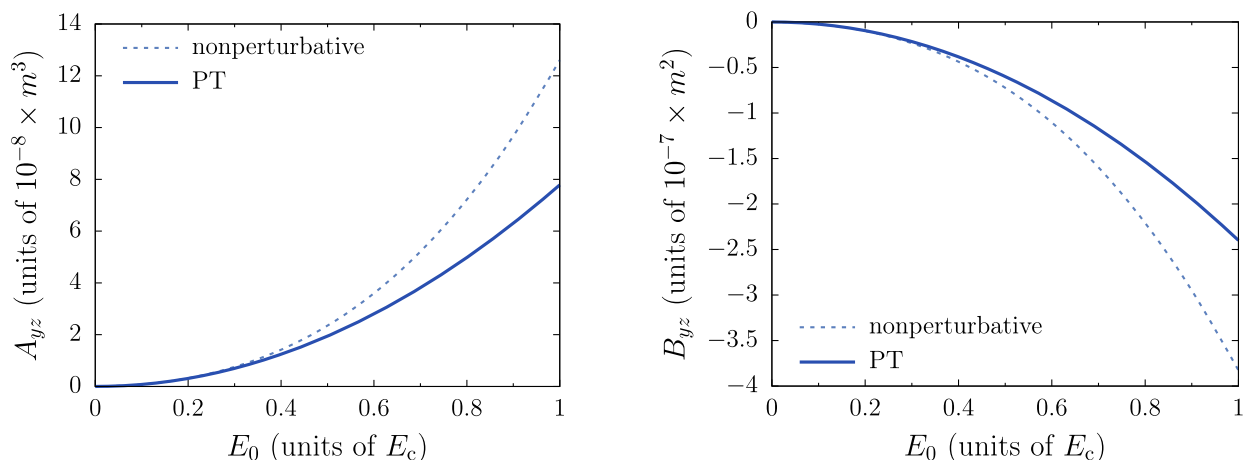
FIG. 4.   Coefficients A_{yz} and B_{yz} as functions of the field amplitude E_0 of the Sauter pulse (10) for $\tau = 1.0m^{-1}$. The results were obtained by means of the nonperturbative expression (13) and within perturbation theory to second order in E_0.

It turns out that in scalar QED the general expression for the vertex contribution is similar to the second term in Eq. (5). It reads

$$n_{\mathbf{k},\lambda}^{(\mathrm{sc})} = e^2 \sum_{n,m} \left| \int d^4x f_{\mathbf{k},\lambda,\mu}^*(x)_+ \varphi_n^*(x) \overleftrightarrow{\partial^\mu}_- \varphi_m(x) \right|^2, \quad (16)$$

where $\varphi_1 \overleftrightarrow{\partial^\mu} \varphi_2 \equiv \varphi_1(\partial^\mu \varphi_2) - (\partial^\mu \varphi_1)\varphi_2$. The quantum numbers n and m correspond to momentum only. In the case of a spatially homogeneous background, the solutions of the Klein-Fock-Gordon equation can be represented as

$$\zeta \varphi_n(x) = \zeta \varphi_{\mathbf{p}}(x) = \frac{1}{(2\pi)^{3/2}} e^{\zeta i \mathbf{p}\mathbf{x}} \zeta \chi_{\mathbf{p}}(t). \quad (17)$$

Then Eq. (16) takes the following form,

$$\frac{(2\pi)^3}{V} n_{\mathbf{k},\lambda}^{(\mathrm{sc})}$$
$$= \frac{\alpha}{4\pi^2} \frac{1}{k^0} \int d\mathbf{p} \left| \int dt_+ \chi_{\mathbf{p}}^*(t) e_\lambda^*(2\mathbf{p} + \mathbf{k})_- \chi_{-\mathbf{p}-\mathbf{k}}(t) e^{ik^0 t} \right|^2, \quad (18)$$

which represents a scalar-QED version of Eq. (13). We assume that $(\mathbf{e}_\lambda, \mathbf{k}) = 0$. The leading $1/k_0^3$ contribution can be evaluated exactly similarly to the spinor-QED calculations outlined in Appendix A [see also Eqs. (B1)–(B3)]. One obtains

$$A_{\mathbf{n},\lambda}^{(\mathrm{sc})} = \frac{\alpha}{8\pi^5} \int d\mathbf{p} \frac{(\mathbf{p}, \mathbf{e}_\lambda)^2 p_0^2(\mathbf{P})}{[p_0^2(\mathbf{P}) - (\mathbf{P}, \mathbf{n})^2]^2} n_{\mathbf{p}}^{(\mathrm{sc})}(1 + n_{\mathbf{p}}^{(\mathrm{sc})}), \quad (19)$$

where $n_{\mathbf{p}}^{(\mathrm{sc})}$ is a number density of bosons produced. One observes that in the spinor case, there is also an additional factor of 2 corresponding to the spin degeneracy and the integrand involves $(\mathbf{P}, \mathbf{e}_\lambda)$ instead of $(\mathbf{p}, \mathbf{e}_\lambda)$. The latter point will not be important as we will focus on the case $(\mathcal{A}_0, \mathbf{e}_\lambda) = 0$. Note that the number density of particles becomes identical in spinor and scalar QED in the realistic regime $E_0 \ll E_c$, $\tau \gg m^{-1}$, $|eE_0|\tau \gg m$ [53]. The factor $1 + n_{\mathbf{p}}^{(\mathrm{sc})}$ reflects the statistics of Bose particles, cf. Eq. (14). In what follows, this factor will be completely inessential as the number density of particles is much smaller than unity in the regime of interest. We underline that Eqs. (14) and (19) were derived independently without any *ad hoc* prescriptions.

Although $B_{\mathbf{n},\lambda}$ can be obtained numerically by the subtraction scheme, we will need the results in the realistic domain, where our direct computations become very time consuming. To overcome this obstacle, we will obtain closed-form expressions for $A_{\mathbf{n},\lambda}$ and $B_{\mathbf{n},\lambda}$ within the WKB approach. Since the spin effects are unimportant here, it is

sufficient to carry out the WKB calculations in the case of scalar QED, which is a subject of the next section.

VI. WKB ANALYSIS

As was stated above, we focus on the realistic domain of the field parameters $E_0 \ll E_c$, $\tau \gg m^{-1}$, $|eE_0|\tau \gg m$, where the WKB approximation is well justified. As we know the asymptotic behavior of the in solutions for $t \le t_{\mathrm{in}}$, we can easily calculate the contribution from the region $(-\infty, t_{\mathrm{in}}]$. The wave functions for $t > t_{\mathrm{in}}$ can be constructed approximately. The leading $1/k_0^3$ term comes from the region $[t_{\mathrm{out}}, +\infty)$. To evaluate it, one should decompose the in solutions in Eq. (18) in terms of the out solutions and use the asymptotic behavior of the latter. Within the WKB approach, one has to combine the functions with different signs of the energy when crossing the Stokes line since it is the Stokes phenomenon that gives rise to nonzero particle yield and also governs photon emission and absorption examined in this study (see, e.g., Refs. [58,59]). It turns out that both $A_{\mathbf{n},\lambda}$ and $B_{\mathbf{n},\lambda}$ are proportional to $|\alpha_{\mathbf{p}}|^2$, where $\alpha_{\mathbf{p}}$ is the WKB transition amplitude between the positive-energy state with momentum $\mathbf{p}$ and the corresponding negative-energy state (see Appendix B for more details). Obviously, $|\alpha_{\mathbf{p}}|^2$ coincides with $n_{\mathbf{p}}$ from Eq. (14) and with $n_{\mathbf{p}}^{(\mathrm{sc})}$ from Eq. (19) once the WKB approach is applicable. The coefficients $A_{\mathbf{n},\lambda}$ can be calculated quite straightforwardly and read

$$A_{\mathbf{n},\lambda}^{(\mathrm{WKB})} = \frac{\alpha}{8\pi^5} \int d\mathbf{p} \frac{(\mathbf{p}, \mathbf{e}_\lambda)^2 p_0^2(\mathbf{P})}{[p_0^2(\mathbf{P}) - (\mathbf{P}, \mathbf{n})^2]^2} |\alpha_{\mathbf{p}}|^2. \quad (20)$$

This expression immediately follows from Eq. (19) and it is very accurate in the case of realistic field parameters. For instance, if $E_0 = 0.1E_c$, then expression (20) deviates from Eq. (19) on the level of 1% already for $\tau \gtrsim 30m^{-1}$. Although one can directly evaluate the exact formula (19) instead of using semiclassical approximations, it is the WKB technique that allows us to obtain a closed-form expression for $B_{\mathbf{n},\lambda}$. We arrive at (see Appendix B)

$$B_{\mathbf{n},\lambda}^{(\mathrm{WKB})} = \frac{\alpha}{8\pi^5} \int d\mathbf{p} \frac{(\mathbf{p}, \mathbf{e}_\lambda)^2 (\mathbf{P}, \mathbf{n})}{[p_0^2(\mathbf{P}) - (\mathbf{P}, \mathbf{n})^2]^2} |\alpha_{\mathbf{p}}|^2. \quad (21)$$

The explicit form of $|\alpha_{\mathbf{p}}|^2$ in the domain of interest reads

$$|\alpha_{\mathbf{p}}|^2 = e^{-\pi\tau(\omega_+ + \omega_- + 2eE_0\tau)}, \quad (22)$$

where $\omega_\pm = \sqrt{m^2 + p_x^2 + p_y^2 + (p_z \pm eE_0\tau)^2}$.

Note that the integrands in Eqs. (20) and (21) contain the difference $p_0^2(\mathbf{P}) - (\mathbf{P}, \mathbf{n})^2$ in the denominator. Since $|eE_0|\tau \gg m$, one has to cancel the term $(p_z + eE_0\tau)^2$ in this difference in order to maximize the coefficients $A_{\mathbf{n},\lambda}$ and $B_{\mathbf{n},\lambda}$. Accordingly, we will assume $\mathbf{n} = \mathbf{e}_z$.

Furthermore, due to the presence of the factor $(\mathbf{P}, \mathbf{n})$, expression (21) vanishes if one chooses $\mathbf{n} = \mathbf{e}_x$ or $\mathbf{n} = \mathbf{e}_y$. The polarization vector $\mathbf{e}_\lambda$ can now point at any direction in the xy plane as the external background is symmetric, so we choose $\mathbf{e}_\lambda = \mathbf{e}_x$.

To calculate A_{zx} and B_{zx}, one can perform integration in Eqs. (20) and (21) numerically. Nevertheless, in the realistic regime, one can also evaluate the integrals approximately by means of Laplace's method since the main contribution arises from a small vicinity of $\mathbf{p} = 0$ due to the exponential suppression of $|\alpha_{\mathbf{p}}|^2$. One obtains

$$A_{zx} \approx \frac{\alpha}{16\pi^6} m^3 (m\tau)^3 \left(\frac{E_0}{E_c}\right)^{11/2} e^{-\pi E_c/E_0}, \qquad (23)$$

$$B_{zx} \approx -\frac{\alpha}{16\pi^6} m^2 (m\tau)^2 \left(\frac{E_0}{E_c}\right)^{9/2} e^{-\pi E_c/E_0}. \qquad (24)$$

Although these formulas contain the exponential factor which arises in the quantitative analysis of the Sauter-Schwinger mechanism, the factors τ^3 and τ^2 substantially enhance the coefficients. Note that measuring photons emitted along the y axis is a completely unfavorable scenario since $A_{yx} \approx (m/|eE_0\tau|)^4 A_{zx} = \gamma^4 A_{zx} \ll A_{zx}$. Accordingly, for more realistic field parameters, the process of vacuum photon emission predicts a huge number of photons traveling parallel to the electric field. This means that almost isotropic radiation revealed in Ref. [29] can be observed only outside the domain considered here. Finally, we note that the coefficient (24) changes its sign if the probe photon travels in the opposite direction.

As an illustration, we present the coefficient A_{zx} as a function of τ for $E_0 = 0.05E_c$ (see Fig. 5). One observes that the approximate expression (23), which predicts the
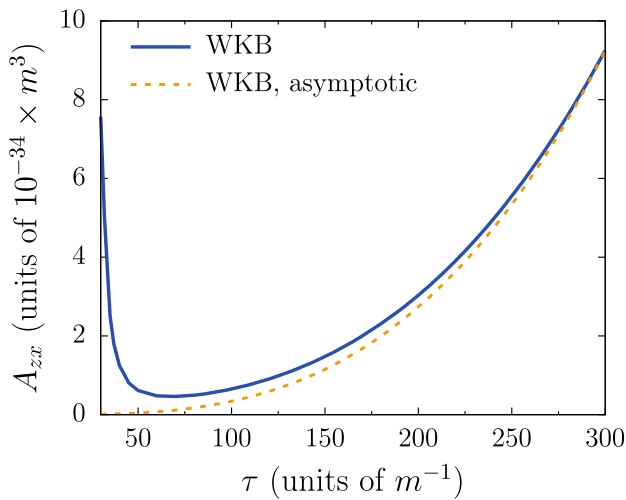

FIG. 5. Coefficient A_{zx} as a function of the pulse duration τ in the case of scalar QED for $E_0 = 0.05E_c$. The asymptotic behavior (dashed line) is given by Eq. (23).

scaling $A_{zx} \sim \tau^3$, is in good agreement with the full WKB calculation.

In what follows, we will examine the experimental scenarios based on measuring either vacuum photon emission or changes in the optical probe beam intensity. We will employ Eqs. (23) and (24) multiplied by a factor of 2. Both these proposals will also be compared with a direct observation of pairs produced, i.e., the Sauter-Schwinger effect itself. To estimate the total particle yield, one can integrate $|\alpha_{\mathbf{p}}|^2$ over $\mathbf{p}$ taking into account the factor $V/(2\pi)^3$. This integration can also be carried out by means of Laplace's method. One finds

$$N^{(\text{pairs})} \approx \frac{1}{(2\pi)^3} (m^3 V)(m\tau) \left(\frac{E_0}{E_c}\right)^{5/2} e^{-\pi E_c/E_0}. \quad (25)$$

VII. DISCUSSION AND EXPERIMENTAL PROSPECTS

Having evaluated the coefficients $A_{n,\lambda}$ and $B_{n,\lambda}$, we can now assess the experimental feasibility of the three following scenarios: (a) direct observation of the Sauter-Schwinger pairs, (b) measuring vacuum radiation, (c) measuring changes in the probe beam intensity. Let us discuss each of these in more detail.

A. Pair production

The total particle yield can be obtained by means of Eq. (25). Let us introduce a laser wavelength and approximate it by $\lambda \approx 2\tau$. Assuming that the laser radiation is tightly focused, we note that the volume factor V is proportional to λ^3. However, taking into account the spatial profile of the external field will definitely reduce the number of pairs since the external field does not have a maximal amplitude in the whole interaction region. To estimate the effect of the spatial inhomogeneities, one can examine the *local* values of the particle yield since the realistic laser wavelength is very large [57]. Moreover, the pair-production process in the nonperturbative regime is mainly governed by the exponential function $\exp[-\pi E_c/|E(x)|]$. One can easily verify that for a profile $E(x) = E_0 \cos(2\pi x/\lambda)$, this exponential contributes only within the vicinity $|x| \lesssim 0.08\lambda$ once $E_0 \lesssim 0.1E_c$. Accordingly, in what follows, we will assume that the effective interaction volume amounts to $V = (0.1\lambda)^3$.

Computing now the number of pairs (25), we will identify the threshold value of the field amplitude E_0 depending on τ by the condition $N^{(\text{pairs})} = 10$. Finally, we point out that expression (25) is quite universal with respect to the choice of the temporal profile of the external field. For instance, in the case of an oscillating background with duration $T = \tau$, one obtains a similar expression which differs from Eq. (25) only by factor $2^{3/2}/\pi \approx 0.9$ (see, e.g., Refs. [57,60–63]).

B. Vacuum emission of soft photons

As was demonstrated above, the major part of the soft photons emitted from vacuum travels parallel to the z axis. The number of photons can be obtained by integrating Eq. (6). Here $d\mathbf{k} = k_0^2 \sin\theta dk_0 d\theta d\varphi$, so the number of signal photons in this scenario reads

$$N^{(\text{vac})} = 2\pi V \sum_\lambda \int_0^{\pi/2} d\theta \sin\theta \int_{k_{\min}^0}^{k_{\max}^0} dk_0 \frac{A_{n,\lambda}}{k_0}, \quad (26)$$

where we imply $\mathbf{n} = \sin\theta \mathbf{e}_x + \cos\theta \mathbf{e}_z$ replacing the integration over φ with the factor 2π. The upper limit regarding the θ integration is inessential as the main contribution arises from a small vicinity of $\theta = 0$. For this reason, we also assume $\mathbf{e}_\lambda = \mathbf{e}_x$ in the expression for $A_{n,\lambda}$ and take into account the second polarization by multiplying the results by a factor of 2. This brings us to the following result,

$$N^{(\text{vac})} \approx \frac{\alpha}{4\pi^5}(m^3 V)(m\tau)\ln\left(\frac{k_{\max}^0}{k_{\min}^0}\right)\left(\frac{E_0}{E_c}\right)^{7/2} e^{-\pi E_c/E_0}. \quad (27)$$

The interval $[k_{\min}^0, k_{\max}^0]$, where one measures the signal photons, is assumed to obey $\ln(k_{\max}^0/k_{\min}^0) = \ln 4$, which corresponds to, e.g., a frequency interval twice as large as the full width of the visible spectrum. The threshold of the process is defined via $N^{(\text{vac})} = 10$, i.e., one has to be able to detect at least ten signal photons. It is already seen that the number of soft photons is suppressed by additional factor E_0/E_c compared to the particle yield (25). In what follows, we will find out how this affects the experimental prospects of this scenario.

C. Probe beam intensity

Here we propose to measure a relative change in the intensity of the probe photon beam, which can be evaluated via

$$\eta \equiv \frac{N^{(\text{ph})}}{N} = \frac{2(2\pi)^3 |B_{zx}|}{q_0^2}, \quad (28)$$

where we will employ Eq. (24). Note that the probe beam is orthogonal to the propagation direction of the lasers that we treat here as a classical background, so the primary laser beams as well as the photons emitted via the tadpole diagram will not obscure the probe quanta. Moreover, the vacuum term (27) is many orders of magnitude smaller than the initial number of probe photons N even if we sum over all spatial directions.

The ratio (28) can be enhanced by choosing a low frequency of the probe photons. We will assume $q_0 = 10^{-6}m$, which corresponds to a wavelength of $2.4\ \mu m$. The realistic threshold of this scenario is set to
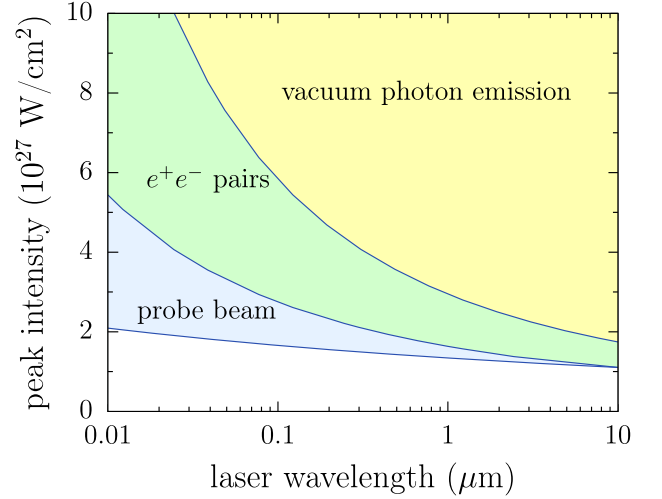

FIG. 6. Threshold values of the laser peak intensity that are necessary for measuring vacuum photon emission (upper curve), the Sauter-Schwinger effect itself (middle curve), and changes in the intensity of the probe photon beam (lower curve).

$\eta = 0.01$, i.e., the relative intensity change should amount to at least one percent. It is reasonable since the uncertainty is proportional to $1/\sqrt{N^{(\text{ph})}}$ while the number of photons can easily be very large.

D. Comparison

In Fig. 6 we present the threshold values of the external field amplitude in terms of the laser intensity for various values of the laser wavelength. As in each of the three scenarios, the signal is proportional to $\exp(-\pi E_c/E_0)$, the curves were found to be stable with respect to the changes of the parameters involved in the pre-exponential factors and threshold values of $N^{(\text{pairs})}$, $N^{(\text{vac})}$, and η, respectively. First, one observes that although the peak intensity corresponding to the field strength E_c is 2.3×10^{29} W/cm², the real threshold of the pair-production process is about two orders of magnitude lower due to the presence of a large preexponential factor (it was examined also, e.g., in Ref. [64]). Second, it turns out that measuring vacuum photon emission is not that promising compared to a direct detection of the Sauter-Schwinger pairs. Note that both of these contributions are proportional to τ^4, so the threshold values of the laser intensity decrease rather rapidly with increasing λ. Nevertheless, the probe-photon technique turns out to be more advantageous, especially for smaller values of λ. Note that from the experimental point of view, it is sufficient to confirm that the intensity of the probe beam changes once it traverses a strong background field, whereas one does not have to determine the actual absolute value of the intensity.

Finally, let us provide several additional remarks concerning the experimental implementation of the three setups. If the external field contains several cycles for a

given half period $\tau = \lambda/2$, the particle yield as well as the number of soft photons will be enhanced by the corresponding factor, which will also slightly lower the position of the curves in Fig. 6. On the other hand, it is crucial to have a unipolar laser background to achieve notable changes in the intensity of the probe photon beam. Further developments in the practical generation of such unipolar pulses (see Ref. [65]), especially in the domain $\lambda \lesssim 0.1 \ \mu$m should make the probe-beam technique an efficient tool for measuring nonperturbative strong-field QED effects. More complex field configurations and the significance of the laser pulse unipolarity will be examined in our future studies.

VIII. CONCLUSION

In this study, we computed the number density of soft photons emitted in the presence of a strong electric background. The main goals were (a) to examine the role of additional (probe) photons in the initial state and (b) to assess the experimental prospects of two proposals with regard to measuring electromagnetic radiation instead of detecting electron-positron pairs. To perform the necessary computations, we employed the Furry picture formalism together with the WKB approach allowing one to investigate a realistic regime of the field parameters. It was demonstrated that the technique which was proposed here and is based on using an additional optical probe photon beam can be utilized in order to lower the pair production threshold although the pure vacuum radiation is unlikely to be detected prior to the onset of the Sauter-Schwinger effect.

Although in the present paper we obtained general closed-form expressions describing stimulated emission and photon absorption in strong external backgrounds and made first quantitative estimates, there are several important aspects which require further research. First, it is highly desirable to analyze the process in more complex external fields incorporating spatial inhomogeneities. Such field configurations may give rise to additional signatures and alter some of the patterns revealed in this study due to the more involved geometry of the setup itself as well as the presence of the magnetic field component. Second, it is very important to more thoroughly inspect the role of the electric-field area of the laser pulses in such backgrounds. These issues are beyond the scope of the present paper and will be explore in future investigations.

ACKNOWLEDGMENTS

APPENDIX A: CALCULATION OF $A_{n,\lambda}$ IN SPINOR QED

Let us first represent expression (13) in the following form

$$\frac{(2\pi)^3}{V} n_{\mathbf{k},\lambda}^{(\text{vac})} = \frac{\alpha}{4\pi^2} \frac{1}{k_0} \sum_{s,s'} \int d\mathbf{p} \left| \frac{a_{s,s'}}{k_0} + b_{s,s'} + \cdots \right|^2. \quad \text{(A1)}$$

Then the coefficient $A_{n,\lambda}$ reads

$$A_{n,\lambda} = \frac{\alpha}{32\pi^5} \sum_{s,s'} \int d\mathbf{p} |a_{s,s'}|^2. \quad \text{(A2)}$$

As was stated in the text, the leading contribution $a_{s,s'}/k_0$ arises from integrating over $t \in [t_{\text{out}}, +\infty)$ in Eq. (13). To perform this integration, one has to express the in solutions in terms of the out ones and make use of the asymptotic behavior of the latter. Here we will need the following scalar products,

$$G(_\zeta|^\kappa)_{\mathbf{p},s,\mathbf{p}',s'} = (_\zeta\varphi_{\mathbf{p},s}, {}^\kappa\varphi_{\mathbf{p}',s'}), \quad \text{(A3)}$$

where $\zeta, \kappa = \pm$. In the case of a spatially homogeneous external background, the one-particle solutions have the form (12) and correspond to conserved values of the spin quantum number s. So the G matrices read

$$G(_\zeta|^\kappa)_{\mathbf{p},s,\mathbf{p}',s'} = \delta_{s,s'} \delta(\zeta\mathbf{p} - \kappa\mathbf{p}') g(_\zeta|^\kappa)_{\mathbf{p},s}. \quad \text{(A4)}$$

The leading-order contribution involving $a_{s,s'}$ comes from the integral over $t \in [t_{\text{out}}, +\infty)$ in Eq. (13), which was also indicated in Ref. [29]. One obtains

$$a_{s,s'} = \frac{i(\bar{u}_{\mathbf{P},s}\gamma^\mu \varepsilon_\mu^* u_{\mathbf{P},s'})}{1 - (\mathbf{P},\mathbf{n})/p_0(\mathbf{P})} g(_+|^+)_{\mathbf{p},s} g^*(_-|^+)_{-\mathbf{p},s'}$$
$$+ \frac{i(\bar{v}_{\mathbf{P},s}\gamma^\mu \varepsilon_\mu^* v_{\mathbf{P},s'})}{1 + (\mathbf{P},\mathbf{n})/p_0(\mathbf{P})} g(_+|^-)_{\mathbf{p},s} g^*(_-|^-)_{-\mathbf{p},s'}, \quad \text{(A5)}$$

where $\mathbf{P} = \mathbf{p} - e\mathcal{A}_0$ and $u_{\mathbf{p},s}$ ($v_{\mathbf{p},s}$) are constant bispinors corresponding to the positive (negative) energy solutions of the free Dirac equation [cf. Eq. (B2) in Ref. [29]]. Taking the mod-square of Eq. (A5), one has to compute standard traces involving bispinors and the gamma matrices. The crucial point here is that in the case of a Sauter profile (10), the g coefficients are known explicitly [35]. For instance,

$$g(_+|^+)_{p,s} = \sqrt{\frac{\omega_-}{\omega_+}}\sqrt{\frac{\omega_+ + p_z + eE_0\tau}{\omega_- + p_z - eE_0\tau}}$$
$$\times \frac{\Gamma(1 + i\omega_+\tau)\Gamma(i\omega_-\tau)}{\Gamma(i\xi_-\tau/2)\Gamma(1 + i\xi_+\tau/2)}, \qquad \text{(A6)}$$

where $\xi_\pm \equiv \omega_+ + \omega_- \pm 2eE_0\tau$. The coefficients with opposite signs yield the number density n_p of the electrons (positrons) produced

$$n_p = |g(_+|^-)_{p,s}|^2 = |g(_-|^+)_{-p,s}|^2. \qquad \text{(A7)}$$

The coefficients with only positive (negative) signs obey

$$|g(_+|^+)_{p,s}|^2 = |g(_-|^-)_{-p,s}|^2 = 1 - n_p. \qquad \text{(A8)}$$

Then straightforward calculations bring us to Eq. (14).

For completeness, we present the explicit form of n_p,

$$n_p = \frac{\sinh(\pi\sigma_+\tau/2)\sinh(\pi\sigma_-\tau/2)}{\sinh(\pi\omega_+\tau)\sinh(\pi\omega_-\tau)}, \qquad \text{(A9)}$$

where $\sigma_\pm \equiv 2eE_0\tau \pm (\omega_+ - \omega_-)$.

APPENDIX B: WKB CALCULATION OF $B_{n,\lambda}$

As was done in Appendix A, it is again convenient to represent the photon number density (18) in the following form,

$$\frac{(2\pi)^3}{V}n_{k,\lambda}^{(sc)} = \frac{\alpha}{\pi^2}\frac{1}{k^0}\int d\boldsymbol{p}(\boldsymbol{p},\boldsymbol{e}_\lambda)^2\left|\frac{a}{k_0} + b + \cdots\right|^2, \qquad \text{(B1)}$$

where a and b depend on $\boldsymbol{p}$. Instead of Eq. (A5), here we have the following *exact* expression for a,

$$a = \frac{i/2}{p_0(\boldsymbol{P}) - (\boldsymbol{P},\boldsymbol{n})}g(_+|^+)_{\boldsymbol{p}}g^*(_-|^+)_{-\boldsymbol{p}}$$
$$+ \frac{i/2}{p_0(\boldsymbol{P}) + (\boldsymbol{P},\boldsymbol{n})}g(_+|^-)_{\boldsymbol{p}}g^*(_-|^-)_{-\boldsymbol{p}}, \qquad \text{(B2)}$$

where the g matrices are defined analogously to Eqs. (A3) and (A4). Performing calculations similar to those outlined in Appendix A, one can first derive expression (19) for $A_{n,\lambda}$,

$$A_{n,\lambda} = \frac{\alpha}{8\pi^5}\int d\boldsymbol{p}(\boldsymbol{p},\boldsymbol{e}_\lambda)^2|a|^2. \qquad \text{(B3)}$$

In fact, these computations are easier as one deals only with scalar functions instead of matrices. The coefficient $B_{n,\lambda}$ should be evaluated via

$$B_{n,\lambda} = \frac{\alpha}{4\pi^5}\int d\boldsymbol{p}(\boldsymbol{p},\boldsymbol{e}_\lambda)^2\text{Re}(a^*b). \qquad \text{(B4)}$$

Within the WKB approximation, one can explicitly construct the solutions $_\zeta\chi_{\boldsymbol{p}}(t)$. Note that it is the Stokes phenomenon which gives rise to nonzero transition amplitudes between the positive-energy continuum and the negative-energy continuum, i.e., to nonzero elements of g matrices with different signs involved in Eq. (B2). Let $t_{\boldsymbol{p}}$ be the time instant where the Stokes line intersects the real axis (see, e.g., Ref. [66]). Then for $t > t_{\boldsymbol{p}}$, the in solutions $_\zeta\chi_{\boldsymbol{p}}(t)$ represent linear combinations of the out solutions determined by the corresponding asymptotic behavior for $t > t_{\text{out}}$. These combinations read

$$_+\chi_{\boldsymbol{p}} = w_{+,\boldsymbol{p}}{}^+\chi_{\boldsymbol{p}} + \alpha_{\boldsymbol{p}}^*w_{-,\boldsymbol{p}}{}^-\chi_{-\boldsymbol{p}}, \qquad \text{(B5)}$$

$$_-\chi_{\boldsymbol{p}} = w_{-,\boldsymbol{p}}{}^-\chi_{\boldsymbol{p}} + \alpha_{\boldsymbol{p}}w_{+,\boldsymbol{p}}{}^+\chi_{-\boldsymbol{p}}, \qquad \text{(B6)}$$

where

$$w_{\pm,\boldsymbol{p}} = \exp\left[\mp i\int_{t_{\text{in}}}^{t_{\text{out}}}p_0(\boldsymbol{p} - e\boldsymbol{\mathcal{A}})dt\right], \qquad \text{(B7)}$$

$$\alpha_{\boldsymbol{p}} = -i\exp\left[2i\int_{t_{\text{in}}}^{t_{\boldsymbol{p}}}p_0(\boldsymbol{p} - e\boldsymbol{\mathcal{A}})dt\right]\frac{\cosh(\pi\beta_{\boldsymbol{p}}\tau/2)}{\sinh(\pi\gamma_{\boldsymbol{p}}\tau)}, \qquad \text{(B8)}$$

$$\beta_{\boldsymbol{p}} = (\omega_+ - \omega_-)\text{sgn}p_z - 2eE_0\tau, \qquad \text{(B9)}$$

$$\gamma_{\boldsymbol{p}} = \sqrt{m^2 + p_x^2 + p_y^2 + (|p_z| + eE_0\tau)^2}. \qquad \text{(B10)}$$

The coefficients in Eqs. (B5) and (B6) correspond to the g matrices, so the products of the g matrices in Eq. (B2) contain the amplitude $\alpha_{\boldsymbol{p}}$. Combining the terms in Eq. (B2), one obtains

$$a = \frac{i}{p_0(\boldsymbol{P})}\frac{\alpha_{\boldsymbol{p}}}{1 - (\boldsymbol{P},\boldsymbol{n})^2/p_0^2(\boldsymbol{P})}. \qquad \text{(B11)}$$

To evaluate b [see Eq. (B1)], one has to take into account integrals over four temporal intervals in Eq. (18); $(-\infty, t_{\text{in}}]$, $(t_{\text{in}}, t_{\boldsymbol{p}}]$, $(t_{\boldsymbol{p}}, t_{\text{out}})$, and $[t_{\text{out}}, +\infty)$. Accordingly, b contains numerous contributions. However, the real part in Eq. (B4) leaves only one of them given in Eq. (21). In the semi-classical approximation, the absolute value of Eq. (B8) coincides with Eq. (22).

[1] H. Euler and B. Kockel, Naturwissenschaften **23,** 246 (1935).
[2] W. Heisenberg and H. Euler, Z. Phys. **98,** 714 (1936).
[3] V. Weisskopf, Kong. Dans. Vid. Selsk., Mat.-Fys. Medd. **XIV,** 6 (1936).
[4] R. Karplus and M. Neuman, Phys. Rev. **80,** 380 (1950); **83,** 776 (1951).
[5] F. Sauter, Z. Phys. **69,** 742 (1931).
[6] J. Schwinger, Phys. Rev. **82,** 664 (1951).
[7] W. Dittrich and H. Gies, Springer Tracts Mod. Phys. **166,** 1 (2000).
[8] G. V. Dunne, in *From Fields to Strings: Circumnavigating Theoretical Physics*, edited by M. Shifman et al. (World Scientific, Singapore, 2005), Vol. 1, pp. 445–522.
[9] G. V. Dunne, Eur. Phys. J. D **55,** 327 (2009).
[10] T. Heinzl and A. Ilderton, Eur. Phys. J. D **55,** 359 (2009).
[11] M. Marklund and J. Lundin, Eur. Phys. J. D **55,** 319 (2009).
[12] A. Di Piazza, C. Müller, K. Z. Hatsagortsyan, and C. H. Keitel, Rev. Mod. Phys. **84,** 1177 (2012).
[13] D. Blaschke, N. T. Gevorgyan, A. D. Panferov, and S. A. Smolyansky, J. Phys. Conf. Ser. **672,** 012020 (2016).
[14] B. King and T. Heinzl, High Power Laser Sci. Eng. **4,** e5 (2016).
[15] B. S. Xie, Z. L. Li, and S. Tang, Matter Radiat. Extremes **2,** 225 (2017).
[16] D. L. Burke, R. C. Field, G. Horton-Smith, J. E. Spencer, D. Walz, S. C. Berridge, W. M. Bugg, K. Shmakov, A. W. Weidemann, C. Bula, K. T. McDonald, E. J. Prebys, C. Bamber, S. J. Boege, T. Koffas, T. Kotseroglou, A. C. Melissinos, D. D. Meyerhofer, D. A. Reis, and W. Ragg, Phys. Rev. Lett. **79,** 1626 (1997).
[17] C. Bamber, S. J. Boege, T. Koffas, T. Kotseroglou, A. C. Melissinos, D. D. Meyerhofer, D. A. Reis, W. Ragg, C. Bula, K. T. McDonald, E. J. Prebys, D. L. Burke, R. C. Field, G. Horton-Smith, J. E. Spencer, D. Walz, S. C. Berridge, W. M. Bugg, K. Shmakov, and A. W. Weidemann, Phys. Rev. D **60,** 092004 (1999).
[18] J. M. Cole et al., Phys. Rev. X **8,** 011020 (2018).
[19] K. Poder et al., Phys. Rev. X **8,** 031004 (2018).
[20] N. Szpak and R. Schützhold, New J. Phys. **14,** 035001 (2012).
[21] F. Fillion-Gourdeau and S. MacLean, Phys. Rev. B **92,** 035401 (2015).
[22] I. Akal, R. Egger, C. Müller, and S. Villalba-Chávez, Phys. Rev. D **93,** 116006 (2016).
[23] V. Kasper, F. Hebenstreit, F. Jendrzejewski, M. K. Oberthaler, and J. Berges, New. J. Phys. **19,** 023030 (2017).
[24] M. F. Linder, A. Lorke, and R. Schützhold, Phys. Rev. B **97,** 035203 (2018).
[25] A. M. Piñeiro, D. Genkina, M. Lu, and I. B. Spielman, New J. Phys. **21,** 083035 (2019).
[26] S. A. Smolyansky, A. D. Panferov, D. B. Blaschke, and N. T. Gevorgyan, Particles **3,** 456 (2020).
[27] P. Solinas, A. Amoretti, and F. Giazotto, Phys. Rev. Lett. **126,** 117001 (2021).
[28] J. W. Yoon, Y. G. Kim, I. W. Choi, J. H. Sung, H. W. Lee, S. K. Lee, and C. H. Nam, Optica **8,** 630 (2021).
[29] A. Otto and B. Kämpfer, Phys. Rev. D **95,** 125007 (2017).
[30] A. Di Piazza, K. Z. Hatsagortsyan, and C. H. Keitel, Phys. Rev. D **72,** 085005 (2005).
[31] I. A. Aleksandrov, G. Plunien, and V. M. Shabaev, Phys. Rev. D **100,** 116003 (2019).
[32] I. A. Aleksandrov, G. Plunien, and V. M. Shabaev, Phys. Rev. D **94,** 065024 (2016).
[33] I. A. Aleksandrov, G. Plunien, and V. M. Shabaev, Phys. Rev. D **96,** 076006 (2017).
[34] I. A. Aleksandrov, G. Plunien, and V. M. Shabaev, Phys. Rev. D **97,** 116001 (2018).
[35] E. S. Fradkin, D. M. Gitman, and S. M. Shvartsman, *Quantum Electrodynamics with Unstable Vacuum* (Springer-Verlag, Berlin, 1991).
[36] A. M. Fedotov and N. B. Narozhny, Phys. Lett. A **362,** 1 (2007).
[37] N. B. Narozhny and A. M. Fedotov, Laser Phys. **17,** 350 (2007).
[38] F. Karbstein and R. Shaisultanov, Phys. Rev. D **91,** 113002 (2015).
[39] H. Gies, F. Karbstein, and C. Kohlfürst, Phys. Rev. D **97,** 036022 (2018).
[40] H. Gies, F. Karbstein, C. Kohlfürst, and N. Seegert, Phys. Rev. D **97,** 076002 (2018).
[41] B. King, H. Hu, and B. Shen, Phys. Rev. A **98,** 023817 (2018).
[42] N. Ahmadiniaz, J. P. Edwards, and A. Ilderton, J. High Energy Phys. 05 (2019) 038.
[43] A. Blinne, H. Gies, F. Karbstein, C. Kohlfürst, and M. Zepf, Phys. Rev. D **99,** 016006 (2019).
[44] F. Karbstein, A. Blinne, H. Gies, and M. Zepf, Phys. Rev. Lett. **123,** 091802 (2019).
[45] I. A. Aleksandrov, A. D. Panferov, and S. A. Smolyansky, Phys. Rev. A **103,** 053107 (2021).
[46] G. Fauth, J. Berges, and A. Di Piazza, Phys. Rev. D **104,** 036007 (2021).
[47] F. Bloch and A. Nordsieck, Phys. Rev. **52,** 54 (1937).
[48] V. B. Berestetskii, E. M. Lifshitz, and L. P. Pitaevskii, *Quantum Electrodynamics* (Elsevier Butterworth-Heinemann, Oxford, 1982).
[49] D. Seipt and B. Kämpfer, Phys. Rev. D **85,** 101701(R) (2012).
[50] A. Ilderton and G. Torgrimsson, Phys. Rev. D **87,** 085040 (2013).
[51] A. Ilderton and G. Torgrimsson, Phys. Lett. B **725,** 481 (2013).
[52] N. B. Narozhny and A. I. Nikishov, Yad. Fiz. **11,** 1072 (1970) [Sov. J. Nucl. Phys. **11,** 596 (1970)].
[53] S. P. Gavrilov and D. M. Gitman, Phys. Rev. D **53,** 7162 (1996).
[54] H. R. Reiss, J. Math. Phys. (N.Y.) **3,** 59 (1962).
[55] A. I. Nikishov and V. I. Ritus, Zh. Eksp. Teor. Fiz. **46,** 776 (1964) [Sov. Phys. JETP **19,** 529 (1964)].
[56] I. A. Aleksandrov and C. Kohlfürst, Phys. Rev. D **101,** 096009 (2020).
[57] D. G. Sevostyanov, I. A. Aleksandrov, G. Plunien, and V. M. Shabaev, Phys. Rev. D **104,** 076014 (2021).
[58] C. K. Dumlu and G. V. Dunne, Phys. Rev. Lett. **104,** 250402 (2010).
[59] C. K. Dumlu and G. V. Dunne, Phys. Rev. D **83,** 065028 (2011).

[60] V. S. Popov, Pis'ma Zh. Eksp. Teor. Fiz. **13**, 261 (1971) [JETP Lett. **13**, 185 (1971)].

[61] V. S. Popov, Yad. Fiz. **19**, 1140 (1974) [Sov. J. Nucl. Phys. **19**, 584 (1974)].

[62] A. Ringwald, Phys. Lett. B **510**, 107 (2001).

[63] G. V. Dunne, Q. H. Wang, H. Gies, and C. Schubert, Phys. Rev. D **73**, 065028 (2006).

[64] S. S. Bulanov, V. D. Mur, N. B. Narozhny, J. Nees, and V. S. Popov, Phys. Rev. Lett. **104**, 220404 (2010).

[65] V. V. Kozlov, N. N. Rosanov, C. De Angelis, and S. Wabnitz, Phys. Rev. A **84**, 023818 (2011).

[66] H. Taya, T. Fujimori, T. Misumi, M. Nitta, and N. Sakai, J. High Energy Phys. 03 (2021) 082.